Biophysical Chemistry 141 (2009) 94–104

Contents lists available at ScienceDirect

Biophysical Chemistry

journal homepage: http://www.elsevier.com/locate/biophyschem

Differential chemical and thermal unfolding pattern of Rv3588c and Rv1284 of *Mycobacterium tuberculosis* — A comparison by fluorescence and circular dichroism spectroscopy

Somnath Mukherjee, Baisakhee Saha, Amit Kumar Das *

Department of Biotechnology, Indian Institute of Technology, Kharagpur, Kharagpur 721302, India

ARTICLE INFO

Article history:
Received 6 November 2008
Received in revised form 30 December 2008
Accepted 1 January 2009
Available online 11 January 2009

Keywords:
Carbonic anhydrase
Circular dichroism
Fluorescence
Stern–Volmer
Transition midpoint ($D_{1/2}$)
Gibb's free energy change (ΔG)

ABSTRACT

The thermal and chemical unfolding pathways of two β carbonic anhydrases, Rv3588c and Rv1284 of *Mycobacterium tuberculosis* have been compared by fluorescence and circular dichroism. Chemical and thermal denaturation of the tertiary and secondary structures of these two ubiquitous enzymes of the pathogen reveals that the unfolding of Rv3588c is mediated through the formation of a molten globule intermediate with depleted tertiary structure. However, Rv1284 directly unfolds from the native to the unfolded state. Calculation of the thermodynamic parameters suggest that overall Rv3588c is more stable than Rv1284. Stern–Volmer analysis together with the fluorescence spectra of the proteins suggest that Trp115 in Rv1284 is more buried than Trp10 in Rv3588c. The tryptophan residues in both the proteins are surrounded by positively charged amino acid residues.

1. Introduction

Amidst vast technical and medical advancement, *Mycobacterium tuberculosis*, the dreaded pathogen of tuberculosis still continues to wreak havoc by claiming several lives with HIV co-infection especially due to its rapidly emerging resistance to many front-line-antimicrobials. The answer to control this deadly claimant lies in the genome of the bug itself which was deciphered by Cole et al. [1]. Subsequent studies by Sassetti et al. [2,3] have attempted to identify genes that are likely to be required for bacterial survival and infection. *Mycobacterium tuberculosis* (H37Rv) contains two such genes *Rv3588c* and *Rv1284*. The *Rv3588c* gene is necessary for growth of *M. tuberculosis* in vivo [4] and thus serves as a potential drug target. Himar1-based transposon mutagenesis in strain H37Rv [3] shows *Rv1284* is essential and its transcription is highly up-regulated under the starvation conditions used to model persistent bacteria [5]. Both *Rv3588c* and *Rv1284* in H37Rv encode for CA (carbonic anhydrase).

An excellent example of convergent evolution is carbonic anhydrase (EC 4.2.1.1) that is ubiquitous in occurrence and plays a major role in catalyzing the reversible hydration of carbon dioxide to form bicarbonate, required for fatty acid biosynthesis, pH homeostasis and other vital physiological functions. Six classes of convergently evolved forms of CA have been described to date — α-form found in animals and some eubacteria [6], β form widely distributed in plants and eubacteria [7], γ-form in an archaebacterium [8], two diatom forms, δ [9] and ζ [10], of which ζ form is apparently a cadmium metalloenzyme; and a carboxysome form, ε [11]. However, Sawaya et al. has shown the carboxysome ε form is a variant of the β family, distinguished by a lack of active site pairing [12].

Both Rv3588c and Rv1284 belong to the β class of CA. The X-ray crystallographic structure of Rv1284 shows that the active site zinc ion is coordinated by one histidine and two cysteine residues, with a fourth coordination site occupied by water or a substrate analogue. In contrast, in Rv3588c, the active site water molecule has been replaced by an aspartate side chain, thereby breaking a salt bridge with a nearby arginine that was a characteristic feature of Rv1284. The active site of Rv3588c is much more solvent exposed in comparison to the active site of Rv1284 that is completely shielded from the solvent. The two CAs exhibit both of the metal coordination geometries that have previously been observed for structures of this family [13].

Protein unfolding reactions have been shown to proceed through a variety of mechanisms [14]. The simplest mechanism is that of a two-state transition, *i.e.* a reaction that proceeds directly from folded to unfolded state without the occurrence of any detectable intermediate. But many studies have demonstrated that folding and unfolding processes of several proteins involve multiple steps that are associated with one or more intermediates [15–17]. Investigation of unfolding pathway of proteins is an intriguing scientific challenge and a wide variety of biophysical methods like fluorescence, CD (circular dichroism) have been employed for this purpose. The typical CD spectra of proteins

* Corresponding author. Tel.: +91 3222 283756; fax: +91 3222 278707, +91 3222 255303, +91 3222 283756.
E-mail address: amitk@hijli.iitkgp.ernet.in (A.K. Das).

0301-4622/$ – see front matter © 2009 Elsevier B.V. All rights reserved.
doi:10.1016/j.bpc.2009.01.002

originating at near UV, far UV and near UV–Vis region form the basis of CD applications to protein structure [18]. Near-UV CD provides a clue about the tertiary structure of protein taking into account the environment of aromatic amino acids, viz. tryptophan, tyrosine, and phenyl alanine, dipole orientation and disulphide linkages whereas the far UV CD estimates the secondary structure of the proteins. The intrinsic fluorescence of proteins arises primarily from the side chains of tyrosine and tryptophan residues and is thus sensitive to side chain participation. Excitation of the protein sample at 295 nm or above (where tyrosine residues do not absorb), makes it is possible to study the fluorescence due to tryptophan residue alone [19]. Though numerous studies have been done on the unfolding, refolding of α CA, no such work on β CA has been reported till date. The present work is the first of its kind for the beta class and is mainly focused on the comparative study of thermal and chemical induced unfolding pathway of these two CAs of *Mycobacterium tuberculosis* by techniques of CD and fluorescence. Quenching studies have also been carried out for both native and the denatured forms with different polar, neutral and ionic quenchers.

2. Experimental details

2.1. Materials

Tris-(hydroxymethyl)-aminomethane (Tris base), dithiotreitol (DTT), Isopropyl β-D-1-thiogalactopyranoside (IPTG), Phenylmethylsulphonyl fluoride (PMSF), leupeptin, pepstatin, aprotinin were purchased from Sigma-Aldrich. pQE30 plasmid DNA and *E. coli* M15 (pREP4) cells were from Qiagen. All the other chemicals were commercial samples of analytical grade.

2.2. Methods

2.2.1. Cloning, overexpression and purification of His_6-Rv3588c and His_6-Rv1284

The open reading frames of *Rv3588c* and *Rv1284* were amplified by PCR from the H37Rv DNA, using the corresponding primer pairs (given in supplementary material) Both the amplicons were cloned into the *Bam*HI and *Hind*III sites of pQE30 vector, transformed in *E. coli* M15 (pRep4) cells and selected on ampicillin, kanamycin plates. The positive clones were verified by DNA sequencing.

The positive clones of Rv3588c and Rv1284 were grown in Luria Broth with 100 μg/ml ampicillin and 25 μg/ml kanamycin at 37 °C for 3 h during which A_{600} reached 0.6, induced with 100 μM IPTG and further grown for 5 h at 37 °C to maximize the overexpression of the recombinant protein in the cytosol. For Rv3588c, cells from 1 l culture were resuspended in buffer A (10 mM Tris–HCl; pH 8.0, 300 mM NaCl and 10 mM imidazole, 10% glycerol) containing 0.1 mM each of leupeptin, pepstatin, aprotinin and 0.02 mM PMSF. The suspension was lysed by ultrasonication in ice and the lysate centrifuged at 14,000 rpm for 40 min. The supernatant was loaded onto Ni-Sepharose High Performance affinity matrix, pre-equilibrated with buffer A. After extensive washing of the column with Buffer A, the protein was eluted with buffer B (10 mM Tris–HCl; pH 8.0, 300 mM NaCl and 300 mM imidazole, 10% glycerol). The eluted protein was subjected to gel exclusion chromatography by using Superdex 75 on a ÄCTAprime plus system (GE Healthcare Biosciences), equilibrated with buffer C (20 mM Tris–HCl; pH 8.0, 150 mM NaCl, 2 mM DTT, 5% glycerol). 2 ml fractions were collected at a flow rate of 1 ml/min. The fractions containing the desired protein were pooled together. The protein coded by Rv1284 was purified similarly.

The concentration of the proteins were estimated by Bradford's method [20] and the purity verified by 15% SDS-PAGE.

2.2.2. Urea induced unfolding of Rv3588c and Rv1284

For investigating the chemical unfolding pathway, the protein samples in buffer C were incubated with different concentrations of urea (0–7.0 M) for 30 min before spectral proceedings because during this time both Rv3588c and Rv1284 were found to be fully unfolded as monitored by the tryptophan fluorescence and CD studies. A freshly prepared 8 M stock solution of urea in buffer was used in each unfolding experiment. The final reaction volume in each case was 1 ml. The concentrations of the proteins were maintained at 0.1 mg/ml throughout all experiments.

2.2.3. Temperature induced unfolding of Rv3588c and Rv1284

The protein samples (0.1 mg/ml) in buffer C were incubated at temperatures from 293 K to 373 K in an increment of 2–5 degrees by temperature controlled bath. For complete unfolding, the samples were allowed to equilibrate for 15 min at each temperature before the respective scans.

The variations in the tertiary and secondary structural elements of Rv3588c and Rv1284 during the chemical and thermal unfolding pathway were analyzed by fluorescence and CD studies. Data of all fluorescence and CD measurements are average of three independent experiments.

2.2.4. Intrinsic steady state fluorescence measurements

Intrinsic tryptophan fluorescence of the native and the denatured samples were monitored using Fluoro Max 3 (Spex Instruments, USA) spectrofluorimeter at 293 K equipped with a temperature controlled bath (NesLab). Emission spectra were recorded from 300–450 nm using 295 nm as the excitation wavelength to selectively excite the single tryptophan residue in both the proteins. A lidded quartz cuvette of 0.1 cm path length was used in all the experiments. Both the excitation and emission bandwidths were set at 1.5 nm. Each spectrum is an average of four scans, and appropriate buffer blanks were subtracted from respective measurements.

2.2.5. Fluorescence quenching

Aliquots of native Rv1284 and Rv3588c were titrated with 5 M stock solution of acrylamide, succinimide, cesium chloride and potassium iodide at 293 K. The spectrum was recorded after each addition and the fluorescence intensities corrected for dilution. To investigate the extent of tryptophan exposure upon denaturation, same procedure was performed with the proteins denatured with 7 M urea. In each case, the ionic strength was maintained by 0.1 M NaCl. The potassium iodide solution was stabilized by 200 μM sodium thiosulphate solution to prevent the formation of I_3^-. The quenching data were analyzed by the classical and modified Stern–Volmer equations (Eqs. (1) and (2)) [19,21]

$$\frac{F_0}{F} = 1 + K_{SV}[Q] \tag{1}$$

$$\frac{F_0}{F} = (1 + K_{SV}[Q])\exp(V[Q]) \tag{2}$$

where F_0 and F are the respective fluorescence intensities corrected for dilution in the absence and presence of the quencher, $[Q]$ is the molar concentration of the quencher, K_{SV} is the collisional or dynamic quenching constant and V is the static quenching constant.

2.2.6. CD spectra measurements

CD studies were performed in a Jasco J-810 spectropolarimeter using 0.1 cm lidded quartz cell cuvette. The secondary and tertiary structural variations were monitored at 190–240 nm and 250–350 nm wavelength ranges respectively. Molar ellipticity at 220 nm was used for secondary structural analyses. A spectral bandwidth of 2 nm with step resolution 0.2 nm, time constant 2 seconds, sensitivity 10 mdeg, scan speed 50 nm/min were used for all measurements. Each spectrum was recorded with an average of 4 scans with subtraction

of appropriate buffer blank. For analysis of secondary structure, DICHROWEB, the online interactive server was used. [22–24]

2.3. Data analysis

2.3.1. Chemical deanturation

Thermodynamic parameters of the urea-induced reversible unfolding process were determined either by two state or three state models as given by Eqs. (3) and (4) respectively.

$$N \leftrightarrow U \tag{3}$$

$$N \leftrightarrow I \leftrightarrow U \tag{4}$$

where N, I and U represent the native, intermediate and the unfolded states of the proteins respectively. The free energy change at equilibrium, ΔG, during the unfolding process was assumed to vary according to the empirical Eq. (5). [25–27]

$$\Delta G = \Delta G^{\circ} - m[D] \tag{5}$$

where ΔG is the standard free energy change, ΔG^0, is the free energy change at zero denaturant concentration, $[D]$ is the denaturant concentration and m is the corresponding slope of a plot ΔG against [D]. The values of ΔG^0 and m were estimated by fitting the fluorescence or CD intensity (S_{obs}) against denaturant concentration, $[D]$ in Eq. (6) for two state process [25], and Eq. (7) for a three state process [28,29].

$$S_{obs} = \frac{S_N + S_U \exp[-(\Delta G_{N\leftrightarrow U} - m_{N\leftrightarrow U}[D])/RT]}{1 + \exp[-(\Delta G_{N\leftrightarrow U} - m_{N\leftrightarrow U}[D])/RT]} \tag{6}$$

$$S_{obs} = \frac{S_N + S_I \exp[-(\Delta G_{N\leftrightarrow I} - m_{N\leftrightarrow I}[D])/RT] + S_U \exp[-(\Delta G_{N\leftrightarrow I} - m_{N\leftrightarrow I}[D])/RT]\exp[-(\Delta G_{I\leftrightarrow U} - m_{I\leftrightarrow U}[D])/RT]}{1 + \exp[-(\Delta G_{N\leftrightarrow I} - m_{N\leftrightarrow I}[D])/RT] + \exp[-(\Delta G_{N\leftrightarrow I} - m_{N\leftrightarrow I}[D])/RT]\exp[-(\Delta G_{I\leftrightarrow U} - m_{I\leftrightarrow U}[D])/RT]} \tag{7}$$

Here S_N, S_I and S_U represent the signal intensities of the native, intermediate and the unfolded states respectively. $\Delta G_{N\leftrightarrow U}$, $\Delta G_{N\leftrightarrow I}$ and $\Delta G_{I\leftrightarrow U}$ are the free energies for the $N\leftrightarrow U$, $N\leftrightarrow I$ and $I\leftrightarrow U$ transitions, $m_{N\leftrightarrow U}$, $m_{N\leftrightarrow I}$ and $m_{I\leftrightarrow U}$ are the corresponding slopes of plot of ΔG against $[D]$. The transition mid point (i.e. the denaturant concentration at which 50% of the protein is unfolded) for the two state process ($D_{1/2(N-U)}$), and the three state process ($D_{1/2(N-I)}$, $D_{1/2(I-U)}$) can be obtained by dividing $\Delta G_{N\leftrightarrow U}$, $\Delta G_{N\leftrightarrow I}$ and $\Delta G_{I\leftrightarrow U}$ by $m_{N\leftrightarrow U}$, $m_{N\leftrightarrow I}$ and $m_{I\leftrightarrow U}$ respectively [27]. The data for the two state and three state processes were respectively fitted directly in Eqs. (6) and (7) by nonlinear least squares analysis to obtain the best fitted values of m. The total free energy change of protein unfolding following the three state model, ΔG_{total}, was determined by adding the $\Delta G_{N\leftrightarrow I}$ and $\Delta G_{I\leftrightarrow U}$. Considering the three state mechanism as two individual two state mechanisms, the fraction of the protein unfolded (F_U) in each step was calculated using the Eq. (8) [30]

$$F_U = \frac{(S_N - S_{obs})}{(S_N - S_U)} \tag{8}$$

2.3.2. Thermal denaturation

The analysis of the thermal denaturation was done using a two-state model as given by Eq. (3). All the steps were completely reversible. The spectral parameters were fitted directly in the Eq. (9) by non linear least square analysis [31]

$$S_{obs} = \frac{S_N + S_U \exp\left(-\frac{\Delta H_{VH}}{R}\left(\frac{1}{T} - \frac{1}{T_m}\right)\right)}{1 + \exp\left(-\frac{\Delta H_{VH}}{R}\left(\frac{1}{T} - \frac{1}{T_m}\right)\right)} \tag{9}$$

where S_{obs} is the observed spectral parameter, $S_N = A_N + B_N T$ and $S_U = A_U + B_U T$ refer to the linear dependence of the native (N) and unfolded (U) state having the slope B_N and B_U respectively, ΔH_{VH} is the apparent change in van't Hoff enthalpy, R is the universal gas constant, T is the temperature in Kelvin and T_m is the melting temperature or the transition midpoint at which 50% of the protein is unfolded. The K was calculated using Eq. (10).

$$K = \frac{(S_{obs} - S_N)}{(S_U - S_N)} \tag{10}$$

The change in standard Gibb's free energy at each temperature was calculated using the values of K as calculated above using the following Eq. (11) [31]

$$\Delta G^{\circ} = -RT \ln K \tag{11}$$

The three-state thermal transition was considered as two individual two-state mechanisms [30]. The calculations for each transition from native to intermediate and intermediate to unfolded states were

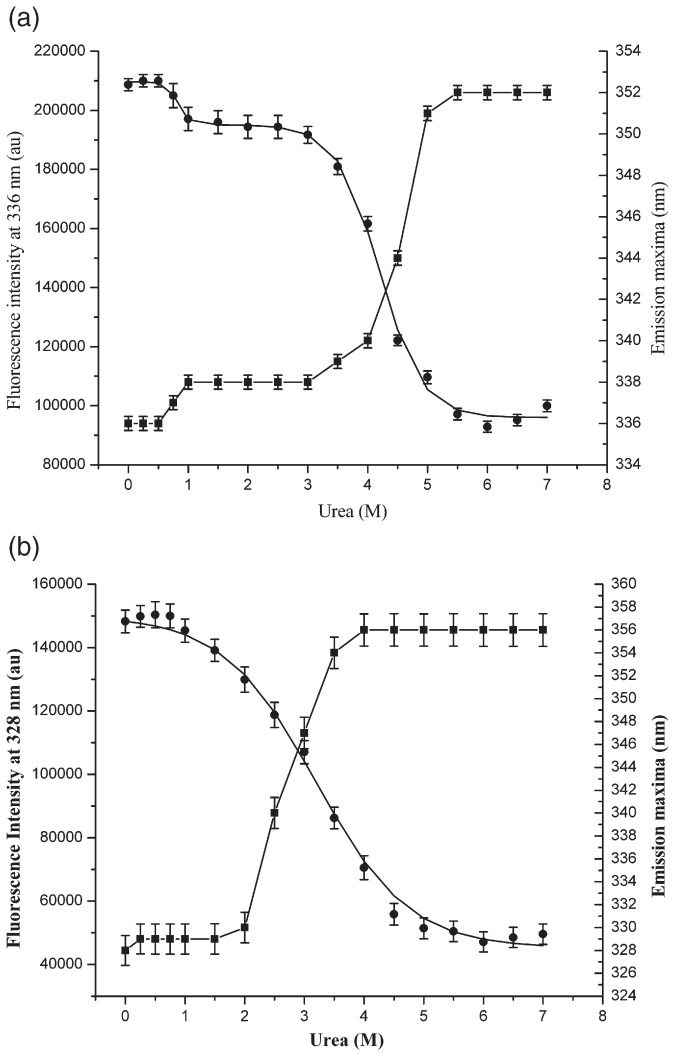

Fig. 1. Urea induced unfolding of Rv3588c and Rv1284 probed using intrinsic tryptophan fluorescence on excitation at 295 nm. (a) Variation of the fluorescence intensity at 336 nm (–●–) and emission maximum (–■–) in Rv3588c. The unfolding isotherm was fitted into a reversible three state model with the fitting parameters: $m_{N\leftrightarrow I}$=2.44±0.02 kJ mol^{-1} M^{-1}, $m_{I\leftrightarrow U}$=5.1±0.05 kJ mol^{-1} M^{-1} (b) Variation of the fluorescence intensity at 328 nm (–●–) and emission maximum (–■–) in Rv1284. The unfolding isotherm was fitted into reversible two state model with the fitting parameter $m_{N\leftrightarrow U}$=5.30±0.06 kJ mol^{-1} M^{-1}.

Table 1
The ΔG values of urea-induced unfolding of Rv3588c and Rv1284, monitored by intrinsic tryptophan fluorescence

Urea (M)	Rv3588c	Rv1284
	ΔG_{total} (kJ mol^{-1})	ΔG_{total} (kJ mol^{-1})
0	24.95±1.18	17.25±1.74
0.25	23.58±1.13	15.93±1.64
0.5	22.22±1.12	14.60±1.00
0.75	20.85±1.00	13.28±0.96
1.0	19.48±1.00	11.95±0.74
1.5	16.75±0.99	9.30±0.45
2.0	14.01±0.85	6.65±0.39
2.5	11.28±0.50	4.0±0.19
3.0	8.54±0.47	1.35±0.06
3.5	5.81±0.33	−1.3±0.20
4.0	3.07±0.33	−3.95±0.42
4.5	0.34±0.09	−6.60±0.68
5.0	−2.4±0.17	−9.25±0.85
5.5	−5.14±0.21	−11.90±0.98
6.0	−7.87±0.67	−14.55±1.14
6.5	−10.61±0.98	−17.20±1.45
7.0	−13.34±1.10	−19.85±1.87

The chemical unfolding of Rv3588c followed a reversible three state model while that of Rv1284 was reversibly biphasic. The ΔG_{total} of Rv3588c was obtained by adding $\Delta G_{N\leftrightarrow I}$ and $\Delta G_{I\leftrightarrow U}$.

done using Eqs. (9)–(11). All the data sets are averages of three independent experiments. The curve fittings in the data analysis were performed using MICROSOFT ORIGIN 6.1 software.

3. Results

3.1. Cloning, purification of His_6-Rv3588c and His_6-Rv1284

PCR amplification of *Rv3588c* and *Rv1284* from *M. tuberculosis* H37Rv genomic DNA yielded amplicons of 621 and 489 bp. The fragments were cloned into the pQE30 expression vector and transformed into *E. coli* M15 (pREP4) cells. The clones were verified by DNA sequencing. His_6-Rv3588c and His_6-Rv1284 were purified by Ni-Sepharose followed by gel exclusion chromatography. Both the proteins were obtained as monomers after gel exclusion experiments (plot not shown). About 20 mg of purified His_6-Rv3588c and 40 mg of purified His_6-Rv1284 were obtained per litre of culture. As analyzed by SDS-PAGE, His_6-Rv3588c and His_6-Rv1284 were estimated to be >95% homogeneous with molecular weight of 23 kDa and 19 kDa respectively.

3.2. Urea induced unfolding of Rv3588c and Rv1284 monitored by fluorescence

The intrinsic fluorescence for the native Rv3588c and Rv1284 was characterized by emission maxima at 336 nm and 328 nm respectively.

In Rv3588c, the progressive loss in the intrinsic fluorescence intensity at the emission maximum of 336 nm occurred in two steps (Fig. 1a). Initially there was a significant reduction of the fluorescence

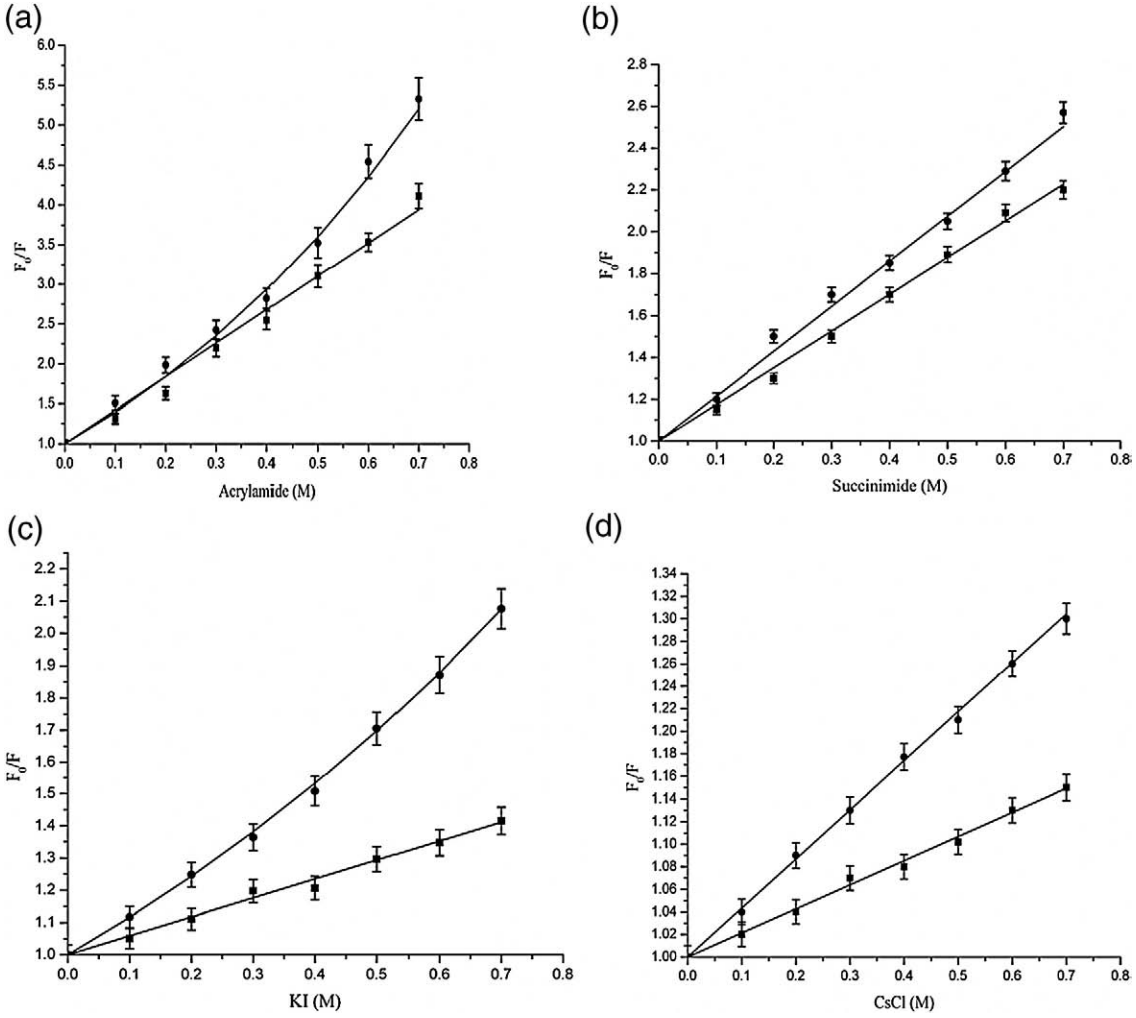

Fig. 2. Stern–Volmer plots of native and denatured Rv3588c: Plot of F/F_0 vs. molar concentration of (a) acrylamide, (b) succinimide, (c) KI, (d) CsCl. (–■–) and (–●–) represent native and denatured proteins respectively.

Table 2
Dynamic and Static Quenching Constants of native and denatured Rv3588c and Rv1284 for different quenchers

Proteins	States	Acrylamide		Succinimide		Cesium chloride		Potassium iodide	
		K_{SV} (M^{-1})	V (M^{-1})	K_{SV} (M^{-1})	V	K_{SV} (M^{-1})	V	K_{SV} (M^{-1})	V (M^{-1})
Rv3588c	Native	4.20±0.42	–	1.75±0.2	–	0.25±0.02	–	0.59±0.07	–
	Denatured	5.00±0.49	0.78±0.08	2.18±0.19	–	0.46±0.05	–	0.84±0.09	0.63±0.07
Rv1284	Native	2.46±0.25	–	1.13±0.11	–	0.26±0.03	–	0.46±0.05	–
	Denatured	5.29±0.51	–	4.46±0.43	–	0.55±0.06	–	0.76±0.02	–

intensity in the presence of 0.75 M urea which further decreased up to 1.0 M urea. The fluorescence intensity almost remained unperturbed up to 3.0 M urea indicating the formation of a stable intermediate from 1.0 M to 3.0 M urea. Further increase in urea concentration from 4.5 M to 5.0 M leads to drastic loss in the intensity in progressive manner. The second transition was essentially complete at 4.5 M urea after which no significant drop in the fluorescence intensity was noticed. Only 20% of the macromolecules were in the folded form (Eq. (8)). The emission maximum (λ_{max}) also suffered a concomitant red shift with increase in denaturant concentration. The first bathochromic shift by 2 nm was observed at 0.75 M urea. At 1.0 M urea, there was another red shift by 2 nm. However after this, up to 3.0 M urea there was no change in the emission maximum wavelength, as in this range of the denaturant concentration, the local environment of the intrinsic fluorophore was undisturbed. Thereafter, there was a gradual increase in the emission maximum up to 4.0 M urea after which it increased sharply by 11 nm to higher wavelength. The spectrum corresponding to the native protein (λ_{max}=336 nm) is blue-shifted relative to that of the unfolded protein (λ_{max}=352 nm). The urea-induced unfolding isotherm was best fitted

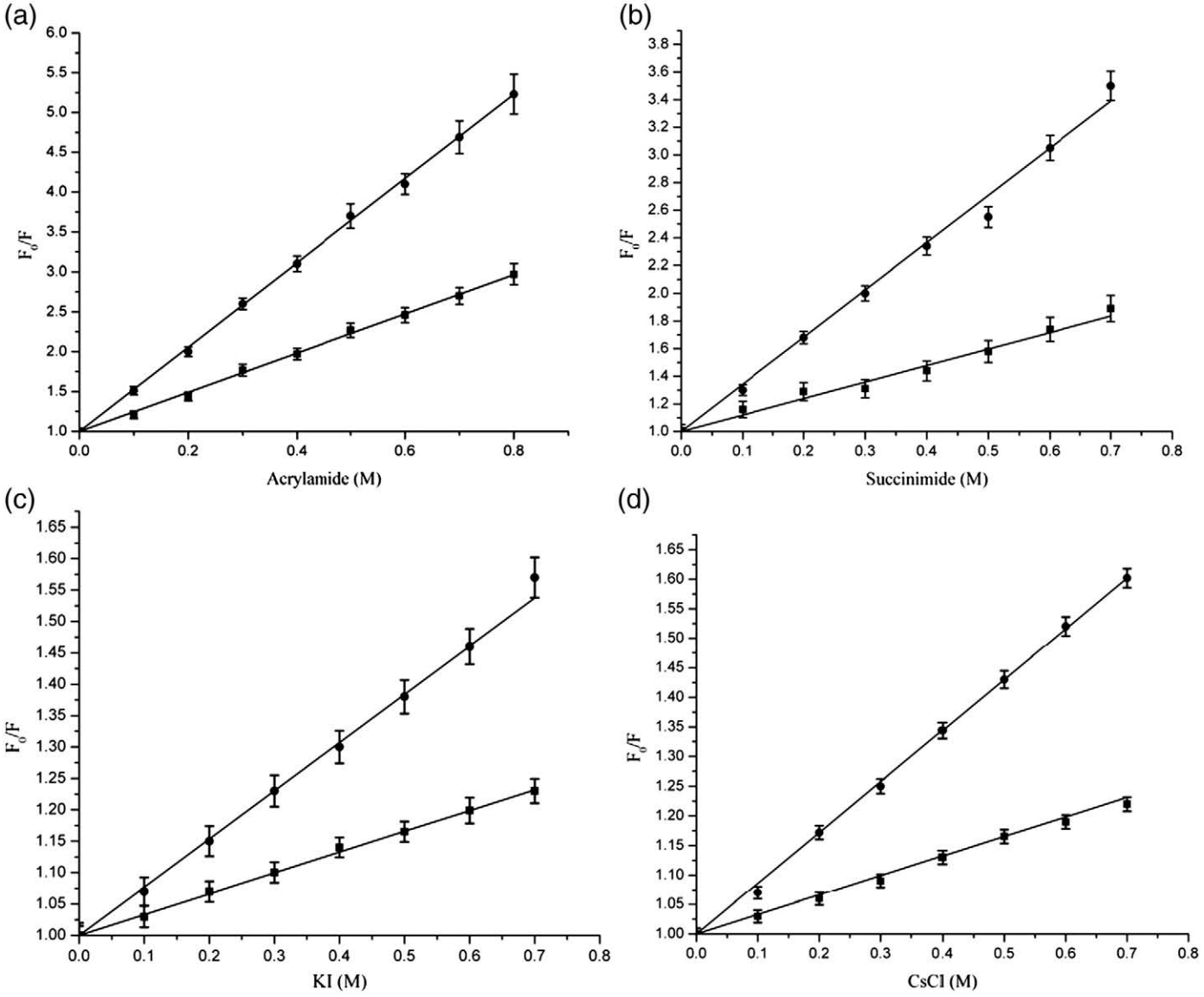

Fig. 3. Stern–Volmer plots of native and denatured Rv1284: Plot of F/F_0 vs. molar concentration of (a) acrylamide, (b) succinimide, (c) KI, (d) CsCl. (–■–) and (–●–) represent native and denatured proteins respectively.

in the three state model given by Eq. (4). The values of ΔG^0 and m were estimated by fitting the intrinsic fluorescence intensity in Eq. (7). The transition mid point of the first transition [$D_{1/2(N-I)}$] and the second transition [$D_{1/2(I-U)}$] of Rv3588c were found to be 0.79±0.08 M and 4.5±0.45 M urea respectively. The unfolding pattern was found to be completely reversible. (Fig. Supp. 1a) The calculated free energy changes (ΔG) of the unfolding of Rv3588c at varying urea concentrations are tabulated in Table 1.

The intrinsic fluorescence for Rv1284 was characterized by a maximum emission wavelength at 328 nm. Urea decreased the intrinsic fluorescence intensity in a concentration dependent fashion with a gradual significant red shift of the emission maxima from 328 nm to 356 nm (Fig. 1b). There was a minimal increase of the emission maximum by 2–3 nm up to 1.5 M urea. However, it increased sharply beyond 2.0 M urea. For example, the emission maximum was 347 nm in the presence of 3.0 M urea. At this denaturant concentration ~76% of the protein was unfolded (Eq. (8)). The progressive loss in the tryptophan fluorescence occurred in a continuous manner without the formation of any detectable intermediate. In this case the unfolding isotherm was best fitted in two-state model given by Eq. (3) and the values of ΔG^0 and m were estimated by fitting the intensity data in Eq. (6). The transition mid point [$D_{1/2(N-U)}$] was found to be 3.25±0.30 M urea. The protein refolded spontaneously upon serial dilution of urea up to 0 M concentration (Fig. Sup. 1b). The free energy changes (ΔG) of the unfolding of Rv1284 at varying urea concentrations are calculated in Table 1.

A plot of ΔG_{total} of Rv3588c and Rv1284 against urea concentrations (result not shown) yielded *x*-axis intercepts of 4.5 and 3 M urea suggesting urea induced unfolding of Rv3588c and Rv1284 occurred spontaneously at urea concentration greater than 4.5 and 3 M respectively. The standard Gibb's free energy changes of unfolding of Rv3588c and Rv1284 were found to be 24.95±1.18 kJ mol^{-1} and 17.25±1.74 kJ mol^{-1} respectively indicating the greater chemical lability of the latter.

3.3. Fluorescence quenching

The microenvironment of the tryptophan residue in Rv3588c and Rv1284 under native and denaturant conditions was investigated by quenching the intrinsic fluorescence of the protein by acrylamide and succinimide, iodide and cesium ions. The quenching results were analyzed by Eqs. (1) and (2).

The Stern–Volmer plots of native Rv3588c and that denatured with 7.0 M urea obtained for different quenchers are shown (Fig. 2) and the corresponding dynamic (K_{SV}) and static quenching constants (V) are listed in Table 2. The collisional quenching constant is greatest for polar uncharged acrylamide (K_{SV}=4.20±0.42 M^{-1}) that can quench both exposed and buried fluorophore followed by succinimide (K_{SV}=1.75±0.20 M^{-1}), iodide (K_{SV}=0.59±0.07 M^{-1}) and cesium (K_{SV}=0.25±0.02 M^{-1}) in the native protein. A linear dependence was inferred between the intrinsic fluorescence intensity of native Rv3588c and the quencher concentration in all the cases suggesting only dynamic quenching in each case. On the other hand, the Stern–Volmer plots for the protein when denatured with 7.0 M urea, showed a positive curvature when quenched by acrylamide and potassium iodide. This indicates that the quenching mechanism in these two cases involve both dynamic and static components. The dynamic quenching constants in denatured protein were maximum for acrylamide (K_{SV}=5.00±0.49 M^{-1}) followed by succinimide (K_{SV}=2.18±0.19 M^{-1}), iodide (K_{SV}=0.84±0.09 M^{-1}) and cesium (K_{SV}=0.46±0.05 M^{-1}). The static quenching constants for acrylamide, and iodide were 0.78±0.08 M^{-1}, and 0.63±0.07 M^{-1} respectively. Upon unfolding with 7 M urea, the extent of quenching increased by a factor of 13% for acrylamide, 8% for succinimide, 30% for potassium iodide and 9% for cesium chloride.

The Stern–Volmer plots of native and denatured Rv1284 are given in Fig. 3. Linear relation between the intrinsic fluorescence intensity of native and denatured Rv1284 and the concentration of acrylamide, succinimide, Cs^+ or I^- suggests only dynamic quenching in each case (Eq. (1)). The corresponding dynamic (K_{SV}) quenching constants are enlisted in Table 2. For native protein, the dynamic quenching constant is greatest for acrylamide (K_{SV}=2.46±0.25 M^{-1}) followed by succinimide, a comparatively bulkier neutral quencher (K_{SV}=1.13±0.10 M^{-1}), the anionic quencher I^- (K_{SV}=0.46±0.05 M^{-1}) and cationic Cs^+ (K_{SV}=0.26±0.03 M^{-1}). In this case also denaturation resulted in a significant increase in intrinsic fluorescence quenching by all the four quenchers. The fluorescence quenching increased by factors of 15%, 11%, 27% and 7% for acrylamide, succinimide, potassium iodide and cesium chloride respectively.

3.4. Structural investigation by circular dichroism

The secondary structure analysis by DICHROWEB predicts that native Rv3588c contains 29% α helix, 21% β strand and 50% random coil. Native

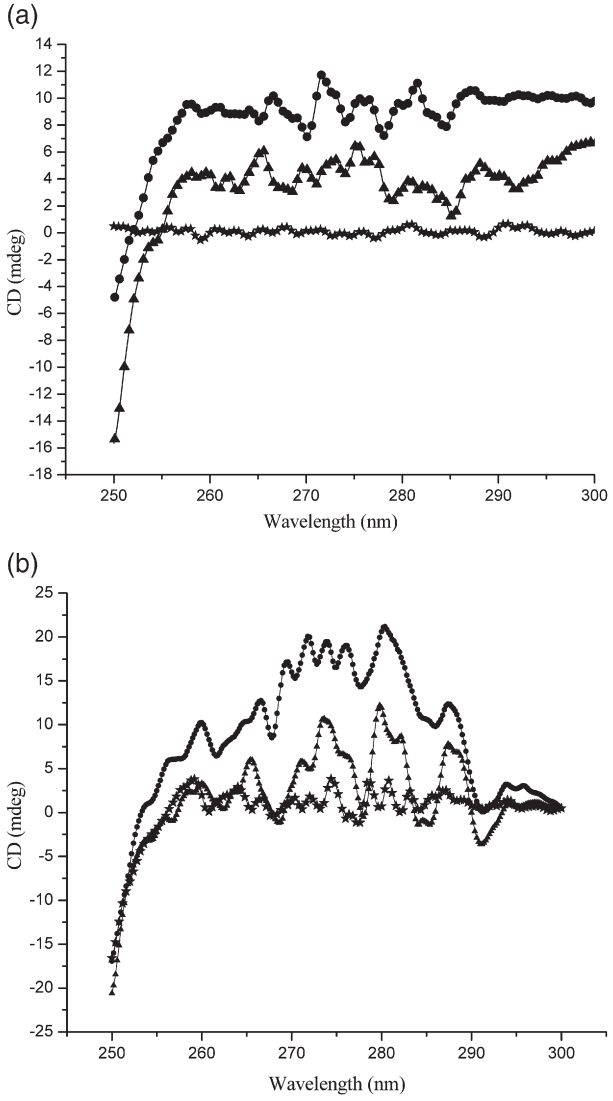

Fig. 4. Urea induced unfolding of tertiary structure of (a) Rv3588c and (b) Rv1284 monitored by near-UV CD spectroscopy. Fig. 4a shows the near-UV CD spectra of native protein (–●–), protein with 0.5 M urea (–▲–), protein with 1.0 M urea (–★–). Fig. 4b shows the near–UV CD spectra of native protein (–●–), protein with 1.5 M urea (–▲–), protein with 3.0 M urea (–★–).

Rv1284 contains 26% α helix, 26% β strand and 52% random coil. These results are in conformity with the secondary structural elements obtained from their crystal structures.

3.5. Urea induced structural transitions monitored by CD spectroscopy

3.5.1. Near-UV circular dichroism

Tertiary structure perturbations of Rv3588c and Rv1284 during chemical unfolding were analyzed from the near-UV circular dichroism spectra of native and the denatured samples.

Between 250–300 nm, native Rv3588c has multiple distinct positive ellipticity peaks at 266.5 nm, 271.7 nm and 281.5 nm. These peaks are attributed to the vibronic states of the aromatic amino acids — phenylalanine, tyrosine and tryptophan respectively. With increase in urea concentration, the ellipticity values decrease indicating gradual unfolding. Fig. 4a depicts the successive changes in the near-UV CD spectra of the protein at various urea concentrations. At 1.0 M urea, the signal peaks disappeared totally indicating a loss in the ordered tertiary structure of the protein.

Native Rv1284 has positive ellipticity peaks at 280.3 nm, 276.1 nm, 273.9 nm, 271.9 nm, 269.5 nm, 266.6 nm, and 259.9 nm, as it contains one tryptophan, three tyrosine and five phenylalanine residues. The CD spectra of Rv1284 at different stages of urea unfolding (Fig. 4b) revealed that the tertiary structure was completely randomized at 3.0 M urea after which no prominent signal in the near-UV CD range of 250–350 nm was obtained.

3.5.2. Far-UV circular dichroism

The secondary structural changes of Rv3588c and Rv1284 were followed by monitoring the far-UV CD spectra as a function of urea concentration The CD spectra of native and fully denatured Rv3588c and Rv1284 recorded from 240–190 nm are given as insets of Fig. 5.

In Rv3588c, increase in urea concentration leads to progressive decrease of CD_{220} (mdeg) values indicating the perturbation in the secondary structure. No significant change in the secondary structure was found up to 3.0 M urea. 6% of the total population was only unfolded. A considerable variation was observed beyond 3.5 M urea. Then the signal intensity progressively decreased with increase in the urea concentration and finally denaturation was essentially complete at 7 M urea. The protein adopted a fully unfolded conformation with no further change in CD_{220} (mdeg) value. It refolded into its original native conformation as monitored by the ellipticity value during refolding experiments (data not shown). The variation in CD (mdeg) at 220 nm with molar concentration of urea (Fig. 5) was well fitted into a two state model (Eq. (3)) and the thermodynamic parameters of unfolding were calculated using Eq. (6). 50% of the molecules were unfolded at 4.57 ± 0.50 M urea. The standard Gibb's free energy change of unfolding was found to be 19.50 ± 1.80 kJ mol^{-1}.

Secondary structure unfolding of Rv1284 follows a similar two state model. Urea unfolded the secondary structure in the concentration dependent manner. There was continuous disruption in the structural elements starting from the low denaturant concentration. However, a sharp decrease of 16% in the signal intensity was observed on treating the protein with 2.5 M urea, leading to a substantial loss of secondary structure. At this concentration of the denaturant, 75% of the protein molecules remain in fully folded native conformation. The apparently undeviated sigmoidal shape of the plot showing the variation of molecular ellipticity monitored at 220 nm with urea concentration (Fig. 5) also retains its exact pattern during refolding experiments. Thus the chemical unfolding of the secondary structure of Rv1284 was fully reversible. The transition midpoint [$D_{1/2(N-U)}$] was calculated to be 3.75 ± 0.33 M urea. The change in standard Gibb's free energy of unfolding of Rv1284 estimated to be 12.85 ± 1.4 kJ mol^{-1}. The variation in Gibb's free energy changes with urea concentration for Rv3588c and Rv1284 were calculated (Table 3). From the plot of ΔG_{total} of Rv3588c and Rv1284 against urea concentrations (plots not shown), the respective *x*-axis intercepts were found to be 4.5 and 3.5 M urea, thereby suggesting that urea induced transitions of the secondary structural elements of Rv3588c and Rv1284 occurred spontaneously at urea concentration above 4.5 and 3.5 M respectively.

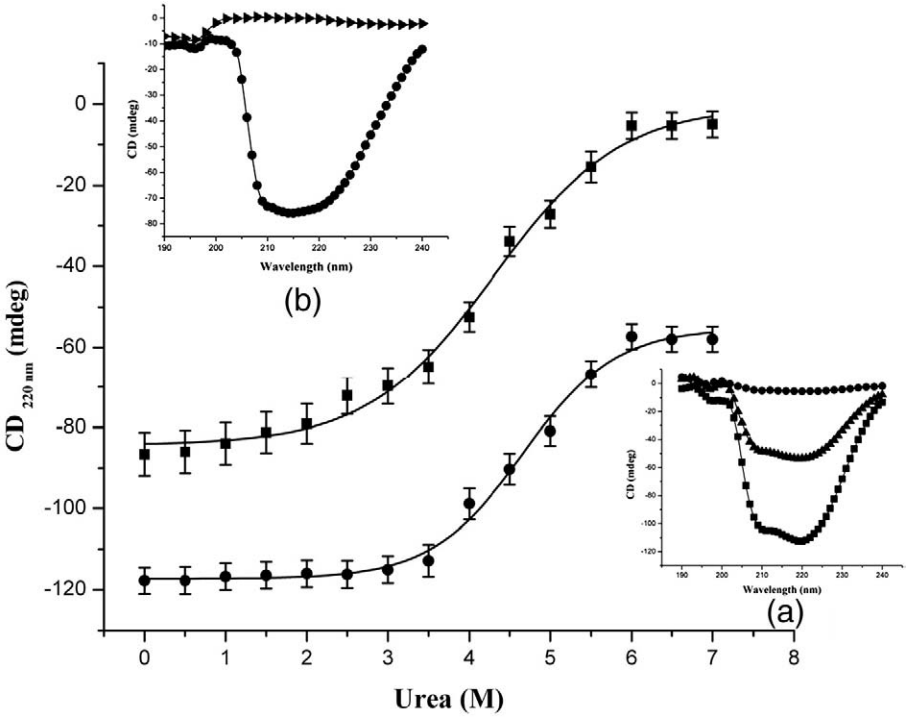

Fig. 5. Urea induced unfolding of secondary structure of Rv3588c and Rv1284. The variation in CD_{220nm} (mdeg) with molar concentration of urea were fitted into reversible two state model both for Rv3588c (–●–) and Rv1284 (–■–) with the fitting parameters m_{N-U} = 4.2 ± 0.03 kJ mol^{-1} M^{-1} and 3.42 ± 0.03 kJ mol^{-1} M^{-1}, respectively. Inset (a) (lower right) shows the far-UV spectra of native (–■–) and denatured (–●–) Rv3588c. Inset (b) (upper left) shows the far-UV spectra of native (–●–) and denatured (–►–) Rv1284.

Table 3
The ΔG values of urea-induced unfolding reaction of Rv3588c and Rv1284, monitored by circular dichroism

Urea (M)	$\Delta G_{N\leftrightarrow U}$ of Rv3588c	$\Delta G_{N\leftrightarrow U}$ of Rv1284
0.0	19.50±1.80	12.85±1.4
0.25	18.82±1.79	12.56±1.3
0.5	17.41±1.65	11.02±1.1
1.0	15.38±1.17	9.18±0.99
1.5	13.21±1.08	7.35±0.76
2.0	11.10±1.00	5.51±0.54
2.5	9.01±0.97	3.68±0.37
3.0	6.97±0.70	1.84±0.18
3.5	4.83±0.49	0.01±0.002
4.0	2.76±0.14	−1.83±0.20
4.5	0.67±0.09	−3.67±0.42
5.0	−1.54±0.12	−5.50±0.64
5.5	−3.66±0.29	−7.34±0.76
6.0	−5.72±0.47	−9.17±0.87
6.5	−7.84±0.82	−11.01±1.29
7.0	−9.91±0.1.12	−12.84±1.30

Both Rv3588c and Rv1284 followed a reversible two state ($N\leftrightarrow U$) model.

3.5.3. Temperature induced unfolding of Rv3588c and Rv1284 monitored by fluorescence

Thermal denaturation experiments were also performed to validate the multistep pathway during unfolding. Fig. Supp. 2a and b present the respective changes in the intensity of the intrinsic fluorophore as a function of temperature when Rv3588c and Rv1284 were excited at 295 nm.

Similar to the chemical unfolding pattern, the thermal denaturation of Rv3588c monitored by fluorescence followed a three state model according to Eq. (4) (Fig. 6). The first unfolding transition was observed between 308–318 K with a 3 nm bathochromic shift of the emission maximum from 336 nm. 25% of the protein was unfolded at this temperature. In the temperature range of 318–323 K, the intensity was almost unchanged, indicative of a stable intermediate. The second unfolding transition was initiated from 328 K whereby there was a significant decrease in the intensity along with a red shift of the emission maximum by 8 nm (Fig. Supp. 2a). The second unfolding transition was essentially complete at 363 K after which no change in the fluorescence signal was noticed. The emission intensity was reduced to 21% of the native state. The thermal unfolding of Rv3588c was fully reversible, and typical refolding profiles match the corresponding unfolding profiles (not shown). Using Eq. (9), ΔH_{VH}, and T_m, accompanying the two transitions were calculated to be 677.54±20.81 kJ mol^{-1}, 312.5±3.1 K and 710.84±23.25 kJ mol^{-1}, 344.8±3.4 K respectively.

The unfolding pattern of Rv1284 was quite different from Rv3588c (Fig. Supp. 2b). Up to 318 K, there was steady decrease in the fluorescence intensity with gradual red shift by 4 nm. At 323 K, a drastic 6 nm red shift was observed with simultaneous quenching of 18% in the quantum yield of the native protein. On raising the temperature to 328 K, the emission intensity again decreased with a further red shift of 10 nm indicating the exposure of the buried tryptophan to a more polar environment upon unfolding, as compared to the native state. With further increment of temperature, the intensity progressively decreased until the denaturation was complete at 353 K. The thermal denaturation was fully reversible and the variation of fluorescence intensity with temperature was sigmoidal in shape without any apparent deviations indicating a two state transition (Fig. 6). The unfolding data was analyzed by using Eq. (9), whereby the ΔH_{VH} and the T_m were 591.89±14.47 kJ mol^{-1} and 324.6±3.2 K respectively. The reversibility of the thermal denaturation for both the proteins was further verified by recording a second thermal

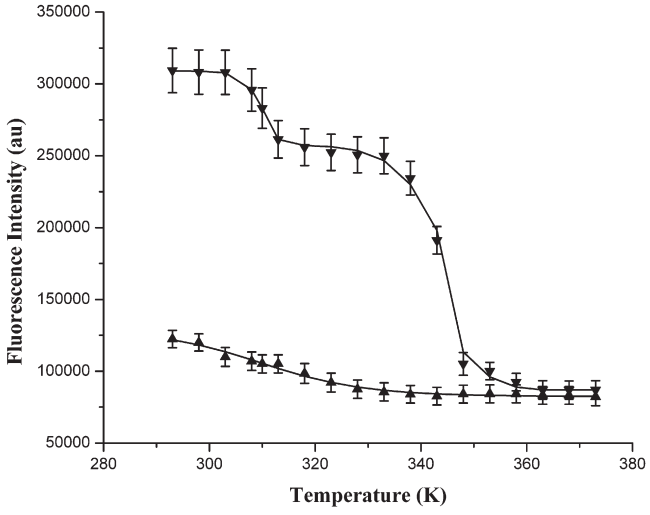

Fig. 6. Thermal unfolding of tertiary structure of Rv3588c and Rv1284 as monitored by the tryptophan fluorescence. The variation in emission intensity for Rv3588c at 336 nm (–▼–) and for Rv1284 at 328 nm (–▲–) with temperature were both fitted into reversible two state model.

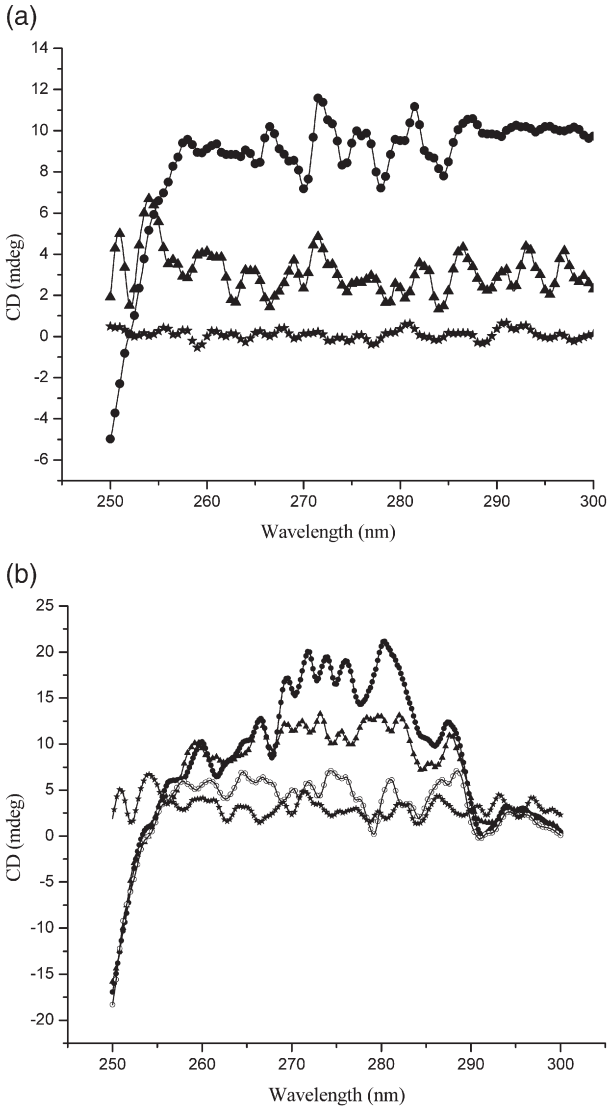

Fig. 7. Thermal unfolding of tertiary structure of (a) Rv3588c and (b) Rv1284 monitored by near-UV CD spectroscopy. Fig. 7a shows the near-UV CD spectra of protein at 293 K (–●–), 300 K (–▲–), 315 K (–★–). Fig. 7b shows the near-UV CD spectra of protein at 293 K (–●–), 300 K (–▲–), 315 K (–○–), and 330 K (–★–).

unfolding profile with the pre-heated samples. The profiles were perfectly superimposable with the corresponding profiles of the samples without pre-heating.

3.6. Temperature induced unfolding of Rv3588c and Rv1284 monitored by circular dichroism

3.6.1. Near-UV CD spectroscopy

Using near-UV CD spectroscopy, the thermal unfolding pattern of the tertiary structure of Rv3588c and Rv1284 was investigated.

Increment of temperature gradually unfolds native Rv3588c. The signal intensities of the positive ellipticities at the specified wavelengths gradually start diminishing (Fig. 7a), which completely disappear at 315 K suggesting the disruption of the tertiary structure.

The tertiary structure of Rv1284 was altered with temperature (Fig. 7b). Initial prominent peaks of the native protein gradually started to decrease in intensity until 330 K. Thereby, with further increase in temperature, no alteration in the CD signal was obtained indicating complete loss of the compact tertiary structure of the protein.

3.6.2. Far-UV CD spectroscopy

The effect of temperature on the secondary structure of CAs of M. tuberculsosis was studied by monitoring the variation of the observed ellipticity at 220 nm with temperature.

The thermal transition of the secondary structure of Rv3588c exhibits a biphasic pattern. The variation in the structural elements, governed by the ellipticity value at 220 nm with temperature was well fitted into N↔U model (Fig. 8). The significant perturbation in the secondary structure was first noticed from 338 K. Denaturation was complete at 368 K with complete disordering of the structural elements (lower right inset of Fig. 8). The pathway was investigated to be completely reversible (Fig. Supp. 3a). The ΔH_{VH}, and T_m, calculated according to Eq. (9), were 780.76±30.28 kJ mol^{-1} and 350±3.5 K respectively.

In Rv1284, the thermal transition up to 323 K was characterized by a little decrease in the ellipticity value without much significant change in the secondary structure. Thereafter the CD values suffered a sharp change in a continuous manner and reached a limiting value at 343 K with complete disruption of the residual secondary structure (upper left inset of Fig. 8). Immediate re-cooling the sample to initial temperature restored 90% of the ellipticity at 220 nm, indicating a relatively high reversibility of the process (Fig. Supp. 3b). Quite similar to the thermal unfolding of the tertiary structure, a two state model also governs the structural transitions of the secondary structure (Fig. 8). The ΔH_{VH} and the T_m from Eq. (9) were calculated to be 611.39± 28.90 kJ mol^{-1} and 332±3.3 K respectively.

The variation in the standard Gibb's free energy with temperature during the structural transitions of these two proteins is tabulated in supplementary section (Table Supp. 1). These values show that at lower temperature, ΔG^0 in Rv1284 is lesser and gradually, with increase in temperature, adopts a more negative value in comparison to that of Rv3588c, indicating that Rv1284 thermally unfolds more spontaneously than Rv3588c.

4. Discussion

Intrinsic tryptophan fluorescence and CD studies have been used in conjunction to probe into the tertiary and secondary structure unfolding of CAs from *Mycobacterium tuberculosis*. Both Rv3588c and Rv1284 contain a single tryptophan residue. Native Rv3588c exhibits λ_{max} of 336 nm while a λ_{max} of 328 nm is observed in case of native Rv1284. These two tryptophan residues (Trp10 in Rv3588c and Trp115 in Rv1284) belong to spectral Class I that represent buried fluorophore [32]. Upon chemical and thermal unfolding, the emission maxima of these two proteins are red shifted suggesting that the fluorophores which were previously located within a less polar environment in the native protein, become solvent exposed in the unfolded state. This is also manifested by the fluorescence intensity of the unfolded protein, which is less than that of the native protein. The rationale behind this conclusion was also supported by the fluorescence quenching.

To analyze the microenvironment and the degree of exposure of the intrinsic fluorophore in the native and the denatured state,

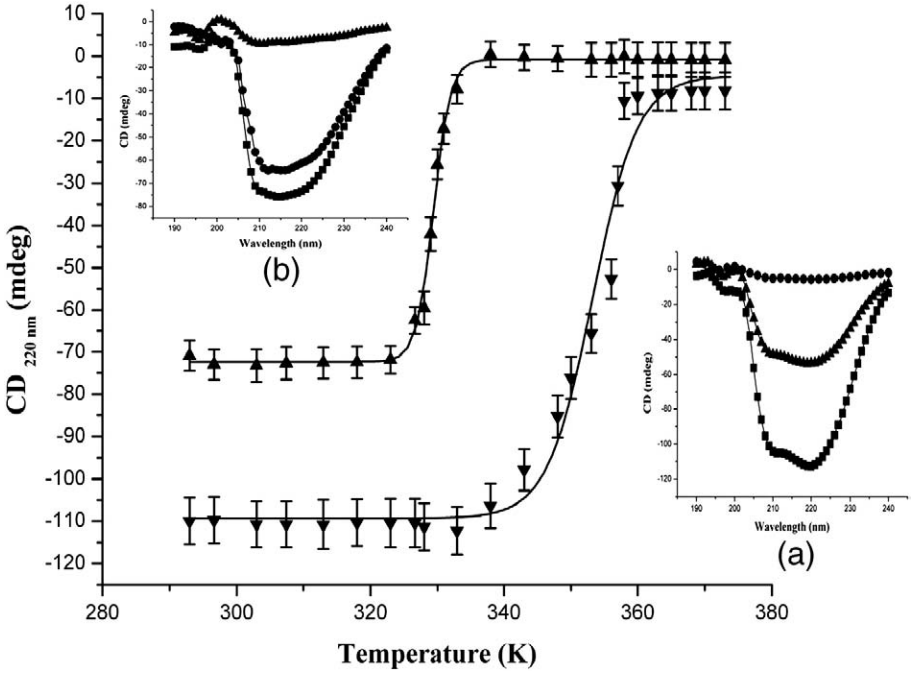

Fig. 8. Thermal unfolding of secondary structure of Rv3588c and Rv1284 monitored by far-UV CD. The variation in $CD_{220\ nm}$ (mdeg) with temperature were fitted into reversible two state model both for Rv3588c (–▼–) and Rv1284 (–▲–). Inset (a) (lower right) shows the far-UV spectra of Rv3588c at 293 K (–■–), 348 K (–▲–), and 368 K (–●–). Inset (b) (upper left) shows the far-UV spectra of Rv1284 at 293 K (–■–), 330 K (–●–) and 343 K (–▲–).

quenching experiments with different chemical quenchers, acrylamide, succinimide, potassium iodide and cesium chloride have been carried out. Acrylamide and succinimide are chemically similar quenchers that differ in their average molecular radii and have been used to study the extent of burial of tryptophan residues in the protein matrix whereas charged quenchers are employed extensively to study the degree of exposure of fluorophores in proteins. The neutral quenchers acrylamide and succinimide can diffuse in the hydrophobic interior of the protein thus quenching even buried residues. On the other hand the charged quenchers cesium (Cs^+) and iodide (I^-) ions have the accessibility of only the surface exposed tryptophan and their extent of quenching largely depends on the nature of charged residues in the vicinity of the fluorophore [33,34]. As the emission maximum of Rv3588c indicates a buried tryptophan, the extent of quenching by different quenchers and their degree of accessibility vary depending on their size and charge. The greatest quenching constant was observed with acrylamide. A lower K_{SV} value for succinimide is explained by its hindered approach to the buried tryptophan due to its larger size and chemical rigidity arising out of its cyclic conformation. The ionic quenchers, Cs^+ and I^-, unable to access the buried tryptophan, exhibit very low values of Stern–Volmer constants. Between Cs^+ and I^- the two, the inability of Cs^+ cesium ions to quench the tryptophan suggest a barrier of positively charged residues around the fluorophore. This is also in agreement with the crystal structure of Rv3588c (PDB entry 1YM3) [13]. The presence of the positive side chains of Lys11 and Lys14 in the immediate neighborhood of Trp10 shields the entry of the cationic quencher (Fig. 9a) [35]. The exposure of the buried tryptophan upon unfolding is also supported by the higher quenching constants of the denatured protein than the native one. Rv1284 also followed a similar pattern. The crystal structure of Rv1284 (PDB entry 1YLK) [13] shows that the single Trp115 resides in the vicinity of Lys102, Arg103 and Arg112 (Fig. 9b) [35]. As inferred from the fluorescence emission maximum, the quenching results also conform to the fact that Trp115 in Rv1284 is more buried in the protein matrix than Trp10 in Rv3588c.

We have observed that on treatment with urea, the tertiary structure unfolding of Rv3588c, follows a three state model while the secondary structure unfolding, occurs through two states. The variation in the fluorescence intensity with molar concentration of urea suggests the formation of an intermediate between 0.79 M to 3.0 M urea. The initial loss of the tertiary structure (first unfolding transition) was at 0.79 ± 0.01 M urea. Near-UV CD studies also suggest that the tertiary structure was diminished at 1.0 M urea. However, no loss of secondary structure (monitored by CD_{220nm} ellipiticity change) was observed at this denaturant concentration. The secondary structural pattern started altering only after 3.0 M urea. This observation concludes the fact that during chemical unfolding of Rv3588c, the loss in tertiary structure precedes the loss in secondary structural elements with the formation of a molten globule intermediate that has a depleted tertiary structure but almost native like secondary structure. The Gibb's free energy change (ΔG) is a measure of the spontaneity of the reaction. The ΔG values of individual steps ($N \leftrightarrow I$) and ($I \leftrightarrow U$) (data not shown) reveal that at low urea concentration, the tertiary structure unfolding from the native to the intermediate step is more spontaneous than the unfolding from the intermediate to the unfolded state. However above 4.5 M urea, the ΔG values for the unfolding from intermediate to unfolded state become more negative than the corresponding values from native to intermediate step due to the instability of the intermediate at high denaturant concentration. In presence of urea, both the tertiary and secondary structures of Rv1284 unfold directly from the native to the unfolded state without the formation of any such intermediate. The transition midpoint is almost same for the tertiary structure and secondary structure unfolding. This suggests the concomitant randomization of the tertiary and secondary structure ruling out the formation of any intermediate.

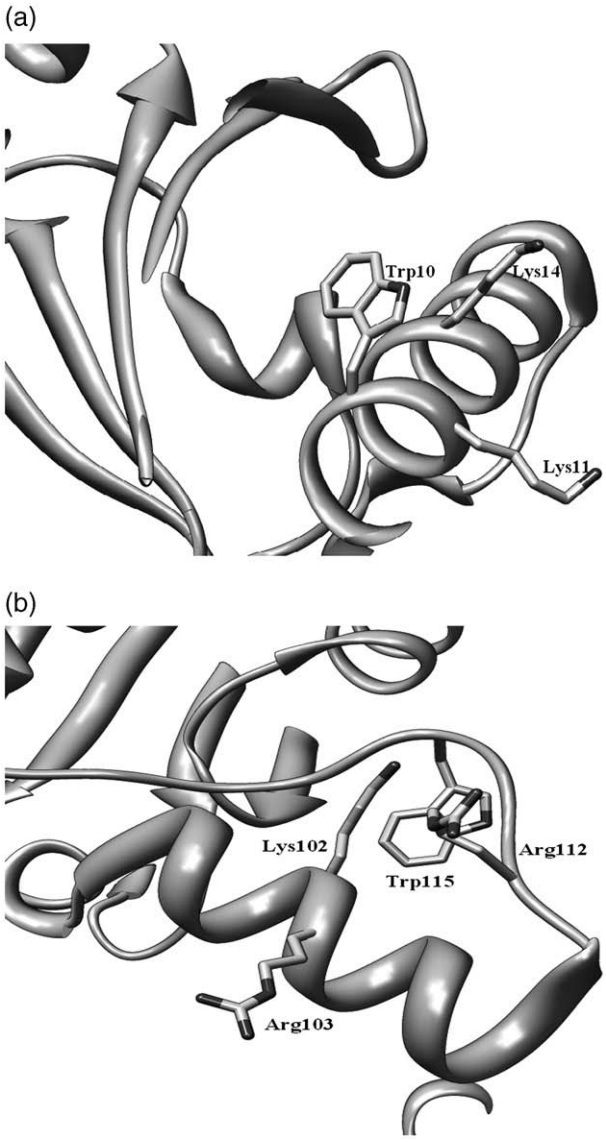

Fig. 9. Microenvironment around the single tryptophan in (a) Rv3588c and (b) Rv1284. In Rv3588c, Trp10 resides amidst Lys11 and Lys14. Trp115 in Rv1284 is surrounded by Lys102, Arg103 and Arg112. The molecular graphics images were produced using the UCSF Chimera package [42].

The thermal unfolding pattern of Rv3588c also asserts the molten globule intermediate. This intermediate was well detected by the intrinsic tryptophan fluorescence. The denaturation profile was well fitted in a three state equation where an intermediate stage was observed in the range of 318–323 K. Conjunction of the observations from the near-UV and far-UV experiments clearly demonstrate the disruption of the tertiary structure starts well before the secondary structure of this mycobacterial enzyme. The molten globule thus formed has a depleted tertiary structural pattern, an observation similar to that obtained from the urea denaturation experiments.

Urea and temperature unfold proteins by different mechanisms. Chemical denaturants like urea, guanidine hydrochloride bind to the peptide bonds and as the protein unfolds more and more peptides are exposed to the denaturants. The electrostatic interactions and the hydrogen bonding pattern are severely impaired [36–39]. The molten globule intermediate with depleted tertiary structure was stable in the range of 1.0–3.0 M urea. This clearly ascertains that this intermediate is stabilized by neither hydrogen bond nor by electrostatic interactions as it is quite stable in moderately high concentrations of urea. But hydrophobic interaction in a protein increases with temperature [40].

The observation that the molten globule was stable in the range of 318–323 K conclusively proves that the principal stabilizing factor behind this intermediate is the hydrophobic interaction. More importantly, this difference in mechanistic action of the denaturants is also reflected in the differing values of the free energy changes, calculated during the structural transitions of these two CAs.

5. Conclusion

A careful comparison of the ΔG^0, ΔH_{VH} and transition midpoint during the unfolding studies of these two mycobacterial enzymes reveals that Rv3588c is more thermally and chemically stable than Rv1284.

Usually, ubiquitous enzymes carrying out the principal metabolic activities are responsible for the sustenance of any microorganism. The tubercle bacillus is an extremely notorious pathogen and can survive in extreme conditions even for months and years. As discussed earlier, carbonic anhydrase is such an important class of enzyme that is responsible for the in vivo growth of the pathogen and upregulated during its starvation conditions. The results obtained from the biophysical studies will be biologically relevant upon knock out studies and simultaneous complementation analyses of Rv3588c and Rv1284 in the pathogen under extreme conditions.

Acknowledgements

The work has been carried out by the financial assistance from Department of Science and Technology and Department of Biotechnology, Government of India. Sincere thanks to Dr. Devrani Mitra, for her kind help and suggestions. S.M. thanks Council of Scientific and Industrial Research, Government of India for individual fellowship.

Appendix A. Supplementary data

Supplementary data associated with this article can be found, in the online version, at doi:10.1016/j.bpc.2009.01.002.

References

[1] S.T. Cole, R. Brosch, J. Parkhill, T. Garnier, C. Churcher, D. Harris, S.V. Gordon, K. Eiglmeier, S. Gas, C.E. Barry III, F. Tekaia, K. Badcock, D. Basham, D. Brown, T. Chillingworth, R. Connor, R. Davies, K. Devlin, T. Feltwell, S. Gentles, N. Hamlin, S. Holroyd, T. Hornsby, K. Jagels, A. Krogh, J. McLean, S. Moule, L. Murphy, K. Oliver, J. Osborne, M.A. Quail, M.A. Rajandream, J. Rogers, S. Rutter, K. Seeger, J. Skelton, R. Squares, S. Squares, J.E. Sulston, K. Taylor, S. Whitehead, B.G. Barrell, Deciphering the biology of *Mycobacterium tuberculosis* from the complete genome sequence, Nature 393 (1998) 537–544.
[2] C.M. Sassetti, E.J. Rubin, Genetic requirements for mycobacterial survival during infection, Proc. Natl. Acad. Sci. U. S. A. 100 (2003) 12989–12994.
[3] C.M. Sassetti, D.H. Boyd, E.J. Rubin, Genes required for mycobacterial growth defined by high density mutagenesis, Mol. Microbiol. 48 (2003) 77–84.
[4] A.S. Covarrubias, T. Bergfors, T.A. Jones, M. Högbom, Structural mechanics of the pH-dependent activity of beta-carbonic anhydrase from *Mycobacterium tuberculosis*, J. Biol. Chem. 281 (2006) 4993–4999.
[5] J.C. Betts, P.T. Lukey, L.C. Robb, R.A. McAdam, K. Duncan, Evaluation of a nutrient starvation model of *Mycobacterium tuberculosis* persistence by gene and protein expression profiling, Mol. Microbiol. 43 (2002) 717–731.
[6] D. Hewett-Emmett, Evolution and distribution of the carbonic anhydrase gene families, EXS 90 (2000) 29–76.
[7] K.S. Smith, C. Jakubzick, T.S. Whittam, J.G. Ferry, Carbonic anhydrase is an ancient enzyme widespread in prokaryotes, Proc. Natl. Acad. Sci. U.S.A. 96 (1999) 15184–15189.
[8] B.E. Alber, J.G. Ferry, A carbonic anhydrase from the archaeon *Methanosarcina thermophila*, Proc. Natl. Acad. Sci. U.S.A. 91 (1994) 6909–6913.
[9] S.B. Roberts, T.W. Lane, F.M.M. Morel, Carbonic anhydrase in the marine diatom *Thalassiosira weissflogii* (bacillariophyta), J. Phycol. 33 (1997) 845–850.
[10] T.W. Lane, M.A. Saito, G.N. George, I.J. Pickering, R.C. Prince, F.M.M. Morel, Biochemistry: a cadmium enzyme from a marine diatom, Nature 435 (2005) 42.
[11] A.K. So, G.S. Espie, E.B. Williams, J.M. Shively, S. Heinhorst, G.C. Cannon, A novel evolutionary lineage of carbonic anhydrase (epsilon class) is a component of the carboxysome shell, J. Bacteriol. 186 (2004) 623–630.
[12] M.R. Sawaya, G.C. Cannon, S. Heinhorst, S. Tanaka, E.B. Williams, T.O. Yeates, C.A. Kerfield, The structure of ε carbonic anhydrasefrom the carboxysomal shell reveals a distinct subclass with one active site for the price of two, J. Biol. Chem. 281 (2006) 7546–7555.
[13] A.S. Covarrubias, A.M. Larsson, M. Högbom, J. Lindberg, T. Bergfors, C. Björkelid, S.L. Mowbray, T. Unge, T.A. Jones, Structure and function of carbonic anhydrases from *Mycobacterium tuberculosis*, J. Biol. Chem. 280 (2005) 18782–18789.
[14] V. Daggett, A.R. Fersht, Is there a unifying mechanism for protein folding? Trends Biochem. Sci. 28 (2003) 18–25.
[15] M. Panda, B.M. Gorovits, P.M. Horowitz, Productive and nonproductive intermediates in the folding of denatured rhodanese, J. Biol. Chem. 275 (2000) 63–70.
[16] B. Nolting, R. Golbik, A.R. Fersht, Submillisecond events in protein folding, Proc. Natl. Acad. Sci. U. S. A. 92 (1995) 10668–10672.
[17] K.W. Plaxco, C.M. Dobson, Time-resolved biophysical methods in the study of protein folding, Curr. Opin. Struct. Biol. 6 (1996) 630–636.
[18] N. Sreerama, R.W. Woody, Computation and analysis of protein circular dichroism spectra, Methods Enzymol. 383 (2004) 318–351.
[19] J.R. Lakowicz, Principles of Fluorescence Spectroscopy, 2nd edn.Kluwer Academic/Plenum Publishers, New York, 1999.
[20] M.M. Bradford, A rapid and sensitive method for the quantitation of microgram quantities of protein utilizing the principle of protein-dye binding, Anal. Biochem. 72 (1976) 248–254.
[21] M.R. Eftink, C.A. Ghiron, Fluorescence quenching studies with proteins, Anal. Biochem. 114 (1981) 199–227.
[22] A. Lobley, B.A. Wallace, DICHROWEB: A website for the analysis of protein secondary structure from circular dichroism spectra, Biophys. J. 80 (2001) 373a.
[23] A. Lobley, L. Whitmore, B.A. Wallace, DICHROWEB: An Interactive Website for the Analysis of Protein Secondary Structure from Circular Dichroism Spectra, Bioinformatics 18 (2002) 211–212.
[24] L. Whitmore, B.A. Wallace, DICHROWEB, an online server for protein secondary structure analyses from circular dichroism spectroscopic data, Nucleic Acid Res. 32 (2004) 668–673.
[25] C.N. Pace, D.V. Laurents, J.A. Thomson, pH dependence of the urea and guanidine hydrochloride denaturation of ribonuclease A and ribonuclease T1, Biochemistry 29 (1990) 2564–2572.
[26] N.A. Morjana, B.J. McKeone, H.F. Gilbert, Guanidine hydrochloride stabilization of a partially unfolded intermediate during the reversible denaturation of protein disulfide isomerase, Proc. Natl. Acad. Sci. U.S.A. 90 (1993) 2107–2111.
[27] K. Flora, J.D. Brennan, G.A. Baker, M.A. Doody, F.V. Bright, Unfolding of acrylodan-labeled human serum albumin probed by steady-state and time-resolved fluorescence methods, Biophys. J. 75 (1998) 1084–1096.
[28] P.R. Bevinton, Data Reduction and Error Analysis for Physical Sciences, McGraw-Hill, New York, 1969.
[29] M.M. Santoro, D.W. Bolen, Unfolding free energy changes determined by the linear extrapolation method. 1. Unfolding of phenylmethanesulfonyl alpha-chymotrypsin using different denaturants, Biochemistry 27 (1988) 8063–8068.
[30] B. Moza, S.H. Qureshi, A. Islam, R. Singh, F. Anjum, A.A.M. Movahedi, F. Ahmad, A unique molten globule state occurs during unfolding of cytochrome c by $LiClO_4$ near physiological pH and temperature: structural and thermodynamic characterization, Biochemistry 45 (2006) 4695–4702.
[31] G. Zoldák, A. Zubrik, A. Musatov, M. Stupák, E. Sedlák, Irreversible thermal denaturation of glucose oxidase from Aspergillus niger is the transition to the denatured state with residual structure, J. Biol. Chem. 279 (2004) 47601–47609.
[32] Y.K. Reshetnyak, E.A. Burstein, Decomposition of protein tryptophan fluorescence spectra into log-normal components. II. The statistical proof of discreteness of tryptophan classes in proteins, Biophys. J. 81 (2001) 1710–1734.
[33] S.S. Lehrer, Solute perturbation of protein fluorescence. The quenching of the tryptophyl fluorescence of model compounds and of lysozyme by iodide ion, Biochemistry 10 (1971) 3254–3263.
[34] A. Grinvald, I.Z. Steinberg, On the analysis of fluorescence decay kinetics by the method of least-squares, Anal. Biochem. 59 (1974) 583–598.
[35] E.F. Pettersen, T.D. Goddard, C.C. Huang, G.S. Couch, D.M. Greenblatt, E.C. Meng, T.E. Ferrin, UCSF Chimera — a visualization system for exploratory research and analysis, J. Comput. Chem. 25 (2004) 1605–1612.
[36] D.R. Robinson, W.P. Jencks, The effect of compounds of the urea-guanidinium class on the activity coefficient of acetyltetraglycine ethyl ester and related compounds, J. Am. Chem. Soc. 87 (1965) 2462–2470.
[37] M. Roseman, W.P. Jencks, Interactions of urea and other polar compounds in water, J. Am. Chem. Soc. 97 (1975) 631–640.
[38] C.N. Pace, Determination and analysis of urea and guanidine hydrochloride denaturation curves, Methods Enzymol. 131 (1986) 266–280.
[39] S.L. Mayo, R.L. Baldwin, Guanidinium chloride induction of partial unfolding in amide proton exchange in RNase A, Science 262 (1993) 873–876.
[40] J.A. Schellman, Temperature, stability and the hydrophobic interaction, Biophys. J. 73 (1997) 2960–2964.